Supplementary Material

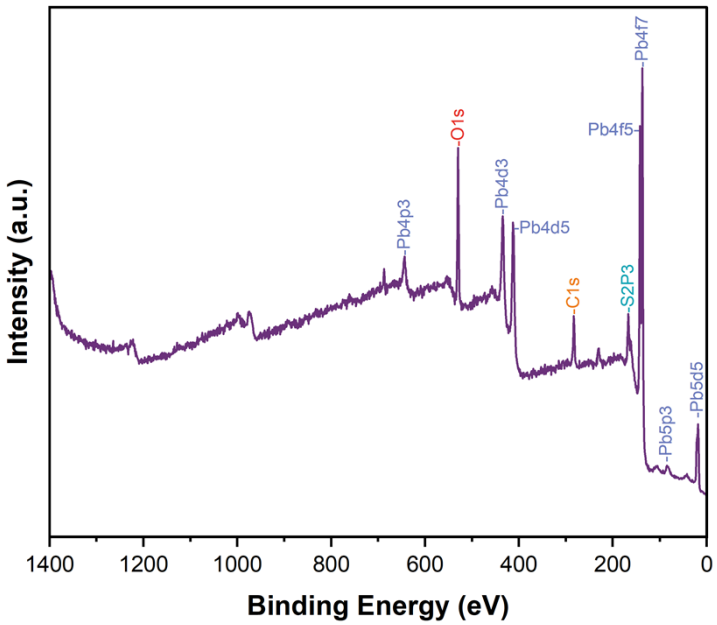

Figure S1. The overall spectrum of SLP raw material XPS.

SPL chemical composition titration method

The chemical composition of spent lead paste (SLP) was analyzed in accordance with the standard method GB/T 23636-2017. The procedures for determining the contents of key lead components are summarized as follows:

1. PbO content

A weighed SLP sample was digested in 5% acetic acid under continuous stirring for 30 minutes. After filtration, the pH of the filtrate was adjusted to 5-6 using ammonia solution. The Pb^{2+} content was then determined via titration with 0.05 mol/L EDTA disodium standard solution, using hexamethylenetetramine as buffer and xylenol orange as indicator.

2. $PbSO_4$ content

The residue obtained from the PbO analysis was dissolved in 25% NaCl solution with stirring for 1 hour. The resulting solution was similarly buffered to pH 5-6 and titrated with 0.05 mol/L EDTA to determine the Pb^{2+} concentration, corresponding to the $PbSO_4$ content.

3. Pb content

The free lead content was determined by treating the sample with a boiling acetic

acid–sodium acetate solution to dissolve non-metallic compounds. The residue containing metallic lead was dissolved in dilute nitric acid, and the Pb^{2+} was titrated at pH 5-6 with 0.02 mol/L EDTA using xylenol orange as indicator.

4. PbO_2 content

The sample was dissolved in nitric acid with the addition of hydrogen peroxide, whereby PbO_2 was reduced and produced peroxide consumed in the reaction. The excess hydrogen peroxide was titrated with potassium permanganate, allowing the calculation of PbO_2 content based on the oxidant consumption.

Thermodynamic calculation process

In Situ Reduction Sulfidation of Lead Paste and Theoretical Thermodynamics

The conversion of lead paste is carried out in a hydrogen peroxide–sulfuric acid system, where PbO_2, PbO, and Pb are transformed into $PbSO_4$. The thermodynamics of the sulfidation conversion process can be summarized by calculating the Pourbaix E-pH diagram of the Pb-S-H_2O_2-H_2O system.

In hydrometallurgical processes, all chemical reactions can be simplified as:

$$aA + nH^+ + ze = bB + cH_2O \tag{1}$$

In the equation, a, n, b, and c represent the stoichiometric coefficients of A, H^+, B, and H_2O in the chemical reaction, respectively, and z is the number of electrons transferred in the reaction. The Gibbs free energy of reaction can be calculated using Eq. (2):

$$\Delta_r G_T^\Theta = c.G_{H_2O,f,T}^\Theta + b.G_{B,f,T}^\Theta - z.G_{e,f,T}^\Theta - n.G_{H^+,f,T}^\Theta - a.G_{A,f,T}^\Theta \tag{2}$$

In Eq. (2), $\Delta_r G_T^\Theta$ represents the standard Gibbs free energy of the chemical reaction shown in (2), and $G_{i,f,T}^\Theta$ denotes the standard Gibbs free energy of formation of various substances at temperature T. According to the van't Hoff isotherm, $\Delta_r G_T$ can be expressed by the following equation:

$$\Delta_r G_T = \Delta_r G_T^\Theta + RT\ln a_B^b/(a_A^a.a_{H^+}^n) \tag{3}$$

Since $-\ln a_{H^+}^n = pH$, Eq. (3) can be rewritten as:

$$\Delta_r G_T = \Delta_r G_T^\Theta + RT\ln(a_B^b/a_A^a) + 2.303nRT.\mathrm{pH} \tag{4}$$

$$\Delta_r G_T = -zFE_T \tag{5}$$

$$\Delta_r G_T^{\Theta} = -zFE_T^{\Theta} \tag{6}$$

Here, E_T and E_T^{Θ} represent the electrode potential and the standard electrode potential of the chemical reaction at a specific temperature, respectively; F is the Faraday constant (F = 96,500 C/mol); R is the molar gas constant (R = 8.314 J/(mol·K)); and a_A and a_B are the activities of species A and B, respectively. By combining Equations (4), (5), and (6), the following relationship can be derived:

$$-zFE_T = -zFE_T^{\Theta} + 2.303RT\lg(a_B^b/a_A^a) + 2.303nRT\mathrm{pH} \tag{7}$$

The chemical reaction shown in Equation (1) can be classified into the following three types based on the substances involved:

(1) Reactions involving H^+ but no electron transfer (i.e., z = 0, n ≠ 0). In this case, Equation (7) can be expressed as:

$$pH = \frac{\Delta_r G_T^{\Theta}}{2.303nRT} - \frac{1}{n}\lg\left(\frac{a_B^b}{a_A^a}\right) \tag{8}$$

(2) For a reaction without H^+ and with electron transfer, that is, a reaction where z≠0 and n=0, equation (7) can be expressed by the following formula:

$$E_T = E_T^{\Theta} - \frac{2.303RT}{z\mathrm{F}}\lg\left(\frac{a_B^b}{a_A^a}\right) \tag{9}$$

(3) Since there are reactions involving H^+ and electron transfer, that is, reactions where z≠0 and n≠0, equation (8) can be expressed by the following formula:

$$E_T = E_T^{\Theta} - \frac{2.303RT}{z\mathrm{F}}\lg\left(\frac{a_B^b}{a_A^a}\right) - \frac{2.303RT}{z\mathrm{F}}n.pH \tag{10}$$

Therefore, as long as the standard Gibbs free energy generated by each substance in the REDOX reaction is obtained, the E-pH diagram of the aqueous solution system at a certain concentration can be plotted according to the equations listed in (8), (9), and (10).

During the transformation process of lead paste, the possible species of lead that may exist include Pb、PbO、PbO_2、$PbSO_4$、Pb^{2+}、Pb^{4+}、PbO_4^{4-}、$HPbO_2^-$、PbO_3^{2-}、Pb_2O_3、Pb_3O_4. The thermodynamic data of the corresponding species are listed **(Table S1)**.

Table S1. Main phases and thermodynamic data existing in the Pb-S-H_2O_2-H_2O system

Species	$G_{f,T}^{\Theta}$(kJ/mol)			Species	$G_{f,T}^{\Theta}$(kJ/mol)		
	298 K	323 K	348 K		298 K	323 K	348 K
Pb	-19.32	-20.97	-22.67	PbO_4^{4-}	-526.32	-518.55	-509.97
PbO	-238.66	-240.37	-242.17	$HPbO_2^-$	-464.38	-465.65	-466.32
PbO_2	-295.88	-297.73	-299.72	PbO_3^{2-}	-439.91	-439.36	-437.80
$PbSO_4$	-964.21	-968.03	-972.05	Pb_2O_3	-531.52	-	-
Pb^{2+}	8.12	8.54	8.58	Pb_3O_4	-781.88	-787.34	-793.24
Pb^{4+}	302.50	-	-	H_2O_2	-220.55	-223.38	-226.38
H^+	6.24	6.64	6.79	H_2O	-306.68	-308.45	-310.42
e	-25.70	-27.75	-29.58	SO_4^{2-}	-928.07	-292.22	-292.61
O_2	-61.13	-66.29	-71.50	H_2S	-82.30	-87.47	-92.71
H_2	-38.93	-42.22	-45.57	SO_2	-371.28	-377.28	-383.61

Note: The "e" in the table represents the electrons that participate in chemical reactions.

Thermodynamic Equations in the Pb-S-H_2O_2-H_2O System

The standard electrode potentials and pH values at different temperatures were calculated. By substituting the calculated standard electrode potentials or pH values into Equation (8), (9), or (10), the thermodynamic equilibrium equations for the Pb-S-H_2O_2-H_2O system at various temperatures can be derived. Based on the equilibrium Equations (6) and (9), the standard electrode potentials and pH values for each reaction at 298 K, 323 K, and 348 K were computed. The possible thermodynamic equations involved in the Pb-S-H_2O_2-H_2O system are summarized in **Table S2**.

Table S2. Electrode reactions and standard electrode potential values at different temperatures in the Pb-S-H_2O_2-H_2O system during the conversion process of SLP.

No.	Reaction	E-pH equation	E_T^{Θ} or pH		
			298K	223K	248K
1	$2H^+ + 2e = H_2$	$E_T = E_T^{\Theta} - \frac{2.303RT}{F} lg(\frac{p_{H_2}}{p^{\Theta}}) - \frac{2.303RT}{F} pH$	0	0	0
2	$O_2 + 4H^+ + 4e = H_2O$	$E_T = E_T^{\Theta} + \frac{2.303RT}{4F} lg(\frac{p_{O_2}}{p^{\Theta}}) - \frac{2.303RT}{F} pH$	1.229	1.208	1.187
3	$Pb + 2H^+ + SO_4^{2-} = PbSO_4 + H_2$	$pH = \frac{-\Delta_r G_T^{\Theta}}{2.303 \times 2RT} + \frac{1}{2} lg(a_{SO_4^{2-}})$	-5.980	-5.931	-5.925
4	$4Pb + 10H^+ + 5SO_4^{2-} = 4PbSO_4 + 4H_2O + H_2S$	$pH = \frac{-\Delta_r G_T^{\Theta}}{2.303 \times 10RT} - \frac{1}{10} lg(\frac{p_{H_2}}{p^{\Theta}}) + \frac{1}{2} lg(a_{SO_4^{2-}})$	-8.951	-8.571	-8.284
5	$Pb + 4H^+ + 2SO_4^{2-} = PbSO_4 + 2H_2O + SO_2$	$pH = \frac{-\Delta_r G_T^{\Theta}}{2.303 \times 4RT} - \frac{1}{4} lg(\frac{p_{H_2S}}{p^{\Theta}}) + \frac{1}{2} lg(a_{SO_4^{2-}})$	-4.230	-4.425	-4.571
6	$Pb + 2H^+ + SO_4^{2-} + H_2O_2 = PbSO_4 + 2H_2O$	$pH = \frac{-\Delta_r G_T^{\Theta}}{2.303 \times 2RT} + \frac{1}{2} lg(a_{SO_4^{2-}} \cdot a_{H_2O_2})$	-37.000	-34.345	-

					32.110
7	$Pb + 2H^+ + H_2O_2 = Pb^{2+} + 2H_2O$	$pH = \frac{-\Delta_r G_T^\ominus}{2.303RT} - \frac{1}{2}lg(a_{Pb^{2+}}) + \frac{1}{2}lg(a_{H_2O_2})$	-33.117	-30.517	- 28.281
8	$PbO + 2H^+ + 2e = Pb + H_2O$	$E_T = E_T^\ominus - \frac{2.303RT}{F}pH$	0.251	0.243	0.235
9	$PbO + 2H^+ + SO_4^{2-} = PbSO_4 + H_2O$	$pH = \frac{-\Delta_r G_T^\ominus}{2.303RT} + \frac{1}{2}lg(a_{SO_4^{2-}})$	-10.223	-9.721	-9.328
10	$PbO_2 + H^+ + 2e = HPbO_2^-$	$E_T = E_T^\ominus - \frac{2.303RT}{2F}lg(a_{HPbO_2^-}) - \frac{2.303RT}{2F}pH$	0.639	0.617	0.592
11	$2PbO_2 + 2H^+ + 2e = Pb_2O_3 + H_2O$	$E_T = E_T^\ominus - \frac{2.303RT}{F}pH$	1.075	-	-
12	$PbO_2 + 4H^+ + 2e = Pb^{2+} + 2H_2O$	$E_T = E_T^\ominus - \frac{2.303RT}{2F}lg(a_{Pb^{2+}}) - \frac{2.303RT}{F}2pH$	1.466	1.460	1.454
13	$PbO_2 + H_2O = PbO_3^- + 2H^+$	$pH = \frac{-\Delta_r G_T^\ominus}{2.303RT} - \frac{1}{2}lg(a_{PbO_3^-})$	15.349	14.567	13.955
14	$PbO + H_2O = HPbO_2^- + H^+$	$pH = \frac{-\Delta_r G_T^\ominus}{2.303RT} - lg(a_{HPbO_2^-})$	15.285	14.530	13.969
15	$3PbO_2 + 4H^+ + 4e = Pb_3O_4 + 2H_2O$	$E_T = E_T^\ominus - \frac{2.303RT}{F}pH$	1.114	1.106	1.098
16	$PbO_2 + SO_4^{2-} + 4H^+ + 2e = PbSO_4 + 2H_2O$	$E_T = E_T^\ominus + \frac{2.303RT}{2F}lg(a_{SO_4^{2-}}) - \frac{2.303RT}{F}2pH$	1.696	1.706	1.718
17	$PbO_2 + H_2O_2 + 2H^+ = Pb^{2+} + 2H_2O + O_2$	$pH = \frac{-\Delta_r G_T^\ominus}{2.303RT} - \frac{1}{2}lg\left(\frac{a_{Pb^{2+}}}{a_{H_2O_2}}\right)$	-14.237	-13.497	-12.85
18	$PbO_2 + Pb + 4H^+ = 2Pb^{2+} + 2H_2O$	$pH = \frac{-\Delta_r G_T^\ominus}{2.303RT} - \frac{1}{2}lg(a_{Pb^{2+}})$	-13.449	-12.444	-11.58
19	$Pb^{2+} + 2e = Pb$	$E_T = E_T^\ominus + \frac{2.303RT}{2F}lg(a_{Pb^{2+}})$	-0.124	-0.135	-0.145
20	$Pb^{2+} + H_2O = PbO + 2H^+$	$pH = \frac{-\Delta_r G_T^\ominus}{2.303RT} + \frac{1}{2}lg(a_{Pb^{2+}})$	6.344	6.893	5.499
21	$Pb^{2+} + 2H_2O = HPbO_2^- + 3H^+$	$pH = \frac{-\Delta_r G_T^\ominus}{2.303RT} - \frac{1}{3}lg\left(\frac{a_{HPbO_2^-}}{a_{Pb^{2+}}}\right)$	9.325	8.772	8.322
22	$Pb^{2+} + H_2O_2 + 2H^+ = Pb^{4+} + 2H_2O$	$pH = \frac{-\Delta_r G_T^\ominus}{2.303RT} - \frac{1}{2}lg\left(\frac{a_{Pb^{4+}}}{a_{Pb^{2+}}}\right)$	-9.721	-	-
23	$Pb^{4+} + 2e = Pb^{2+}$	$E_T = E_T^\ominus - \frac{2.303RT}{zF}lg(\frac{a_{Pb^{2+}}}{a_{Pb^{4+}}})$	1.259	-	-
24	$Pb^{4+} + 2H_2O = PbO_2 + 4H^+$	$pH = \frac{-\Delta_r G_T^\ominus}{2.303 \times 4RT} + \frac{1}{4}lg(a_{Pb^{4+}})$	1.750		
25	$Pb^{4+} + H_2O_2 + 4e = PbO + 2H_2O$	$E_T = E_T^\ominus + \frac{2.303RT}{4F}lg(a_{Pb^{4+}} \cdot a_{H_2O_2})$	2.154	-	-
26	$Pb^{4+} + SO_4^{2-} + 2e = PbSO_4$	$E_T = E_T^\ominus - \frac{2.303RT}{2F}lg(a_{Pb^{4+}} \cdot a_{SO_4^{2-}})$	1.489	-	-
27	$Pb^{4+} + 3H_2O = PbO_3^- + 6H^+$	$pH = \frac{-\Delta_r G_T^\ominus}{2.303 \times 6RT} - \frac{1}{6}lg\left(\frac{a_{PbO_3^-}}{a_{Pb^{4+}}}\right)$	6.283		
28	$HPbO_2^- + 3H^+ + 2e = Pb + 2H_2O$	$E_T = E_T^\ominus + \frac{2.303RT}{2F}lg(a_{HPbO_2^-}) - \frac{2.303RT}{2F}3pH$	0.703	0.708	0.717
29	$2HPbO_2^- + H_2O_2 + 2H^+ = Pb_2O_3 + 3H_2O$	$pH = \frac{-\Delta_r G_T^\ominus}{2.303RT} + \frac{1}{2}lg(a_{HPbO_2^-}^2 \cdot a_{H_2O_2})$	-27.585	-	-
30	$PbO_3^- + 3H^+ + 2e = HPbO_2^- + H_2O$	$E_T = E_T^\ominus - \frac{2.303RT}{2F}lg(\frac{a_{HPbO_2^-}}{a_{PbO_3^-}}) - \frac{2.303RT}{2F}3pH$	1.547	1.551	1.556
31	$PbO_3^- + 6H^+ + 2e = Pb^{2+} + 3H_2O$	$E_T = E_T^\ominus - \frac{2.303RT}{2F}lg(\frac{a_{Pb^{2+}}}{a_{PbO_3^-}}) - \frac{2.303RT}{F}3pH$	2.374	2.394	2.417
32	$2PbO_3^- + 6H^+ + 2e = Pb_2O_3 + 3H_2O$	$E_T = E_T^\ominus + \frac{2.303RT}{F}lg(a_{PbO_3^-}) - \frac{2.303RT}{F}3pH$	2.890	-	-
33	$3PbO_3^- + 10H^+ + 4e = Pb_3O_4 + 5H_2O$	$E_T = E_T^\ominus + \frac{2.303RT}{4F}3lg(a_{PbO_3^-}) - \frac{2.303RT}{4F}10 \times pH$	2.475	2.506	2543
34	$3Pb_2O_3 + 2H^+ + 2e = 2Pb_3O_4 + H_2O$	$E_T = E_T^\ominus - \frac{2.303RT}{F}pH$	1.228	-	-
35	$Pb_2O_3 + 6H^+ + 2e = 2Pb^{2+} + 3H_2O$	$E_T = E_T^\ominus - \frac{2.303RT}{F}3pH$	1.857	-	-
36	$Pb_2O_3 + 2H^+ + 2e = 2PbO + H_2O$	$E_T = E_T^\ominus - \frac{2.303RT}{F}pH$	1.107	-	-
37	$Pb_2O_3 + H_2O_2 + 2H^+ + 4e = 2HPbO_2^- + H_2O$	$E_T = E_T^\ominus - \frac{2.303RT}{4F}lg(\frac{a_{PbO_2}}{a_{H_2O_2}}) - \frac{2.303RT}{2F}pH$	1.018	-	-
38	$Pb_2O_3 + 2SO_4^{2-} + 6H^+ + 2e = 2PbSO_4 + 3H_2O$	$E_T = E_T^\ominus + \frac{2.303RT}{F}lg(a_{SO_4^{2-}}) - \frac{2.303RT}{F}3pH$	2.315	-	-

39	$Pb_3O_4 + 2H^+ + 2e = 3PbO + H_2O$	$E_T = E_T^\Theta - \frac{2.303RT}{F}pH$	1.046	1.037	1.027
40	$Pb_3O_4 + 2H_2O + 2e = 3HPbO_2^- + H^+$	$E_T = E_T^\Theta - \frac{2.303RT}{2F}3lg(c_{HPbO_2^-}) - \frac{2.303RT}{2F}pH$	-0.310	-0.360	-0.420
41	$Pb_3O_4 + 8H^+ + 2e = 3Pb^{2+} + 4H_2O$	$E_T = E_T^\Theta - \frac{2.303RT}{2F}3lg(c_{Pb^{2+}}) - \frac{2.303RT}{F}4pH$	2.171	2.169	2.166
42	$Pb_3O_4 + H_2O_2 + H^+ + 4e = 3HPbO_2^-$	$E_T = E_T^\Theta + \frac{2.303RT}{4F}lg(c_{H_2O_2}) - \frac{2.303RT}{4F}pH$	0.762	0.730	0.694

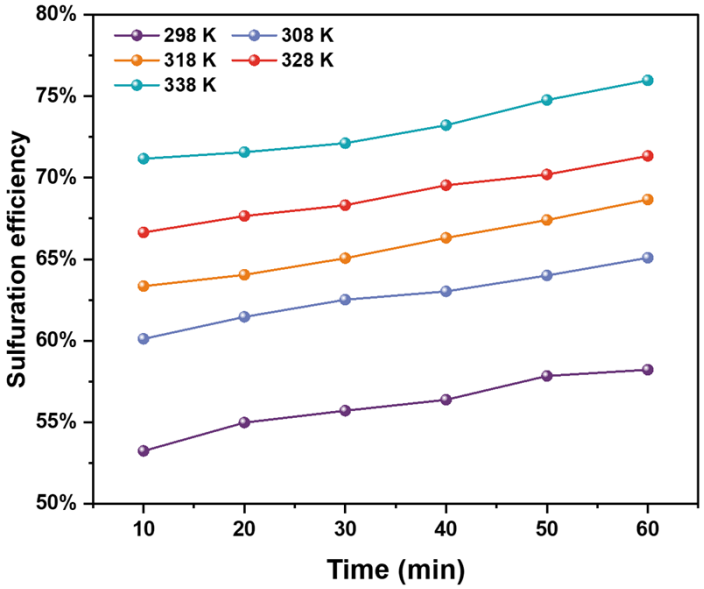

Figure S2. Conventional conversion tests on the vulcanization efficiency of SLP at different temperatures and times

Table S3. The full experimental dataset comprising 399 independent runs used for ANN training and validation.

	Temperature(K)	liquid-Solid ratio(ml/g)	Molar ratio of H_2O_2 to Pb^{4+}	Molar ratio of H_2SO_4 to Pb^{2+}	Ultrasonic power (W)	Sulfuration efficiency
1	328	20	2	1.5	500	98.89%
2	328	20	2	1.5	500	98.23%
3	328	20	2	1.5	500	98.32%
4	348	20	2	1.5	500	98.34%
5	348	20	2	1.5	500	95.76%
6	348	20	2	1.5	500	95.76%
7	328	40	2	1.5	500	86.95%
8	328	40	2	1.5	500	91.16%
9	328	40	2	1.5	500	91.16%
10	348	40	2	1.5	500	85.20%

11	348	40	2	1.5	500	82.16%
12	348	40	2	1.5	500	83.68%
13	338	30	1.75	1.25	500	90.04%
14	338	30	1.75	1.25	500	88.56%
15	338	30	1.75	1.25	500	85.60%
16	338	30	2.25	1.25	500	88.91%
17	338	30	2.25	1.25	500	90.40%
18	338	30	2.25	1.25	500	85.95%
19	338	30	1.75	1.75	500	84.83%
20	338	30	1.75	1.75	500	83.34%
21	338	30	1.75	1.75	500	81.86%
22	338	30	2.25	1.75	500	90.58%
23	338	30	2.25	1.75	500	96.47%
24	338	30	2.25	1.75	500	89.11%
25	338	20	2	1.5	400	91.13%
26	338	20	2	1.5	400	84.12%
27	338	20	2	1.5	400	91.13%
28	338	40	2	1.5	400	83.63%
29	338	40	2	1.5	400	85.03%
30	338	40	2	1.5	400	86.42%
31	338	20	2	1.5	600	92.76%
32	338	20	2	1.5	600	94.21%
33	338	20	2	1.5	600	94.21%
34	338	40	2	1.5	600	86.06%
35	338	40	2	1.5	600	87.49%
36	338	40	2	1.5	600	87.49%
37	328	30	1.75	1.5	500	92.09%
38	328	30	1.75	1.5	500	97.78%
39	328	30	1.75	1.5	500	94.94%
40	348	30	1.75	1.5	500	88.99%
41	348	30	1.75	1.5	500	93.25%
42	348	30	1.75	1.5	500	90.41%
43	328	30	2.25	1.5	500	89.18%
44	328	30	2.25	1.5	500	94.77%
45	328	30	2.25	1.5	500	93.37%
46	348	30	2.25	1.5	500	95.75%
47	348	30	2.25	1.5	500	94.32%
48	348	30	2.25	1.5	500	94.32%
49	338	30	2	1.25	400	89.54%

50	338	30	2	1.25	400	90.89%
51	338	30	2	1.25	400	89.54%
52	338	30	2	1.75	400	92.77%
53	338	30	2	1.75	400	88.48%
54	338	30	2	1.75	400	88.48%
55	338	30	2	1.25	600	87.70%
56	338	30	2	1.25	600	89.16%
57	338	30	2	1.25	600	87.70%
58	338	30	2	1.75	600	91.16%
59	338	30	2	1.75	600	94.14%
60	338	30	2	1.75	600	91.16%
61	338	20	1.75	1.5	500	99.35%
62	338	20	1.75	1.5	500	95.04%
63	338	20	1.75	1.5	500	95.04%
64	338	40	1.75	1.5	500	88.04%
65	338	40	1.75	1.5	500	85.01%
66	338	40	1.75	1.5	500	92.59%
67	338	20	2.25	1.5	500	92.18%
68	338	20	2.25	1.5	500	92.18%
69	338	20	2.25	1.5	500	92.18%
70	338	40	2.25	1.5	500	87.53%
71	338	40	2.25	1.5	500	90.35%
72	338	40	2.25	1.5	500	90.35%
73	328	30	2	1.25	500	91.61%
74	328	30	2	1.25	500	87.36%
75	328	30	2	1.25	500	90.19%
76	348	30	2	1.25	500	82.43%
77	348	30	2	1.25	500	82.43%
78	348	30	2	1.25	500	83.89%
79	328	30	2	1.75	500	91.94%
80	328	30	2	1.75	500	91.94%
81	328	30	2	1.75	500	93.42%
82	348	30	2	1.75	500	96.24%
83	348	30	2	1.75	500	93.40%
84	348	30	2	1.75	500	90.55%
85	338	30	1.75	1.5	400	83.96%
86	338	30	1.75	1.5	400	88.20%
87	338	30	1.75	1.5	400	82.55%
88	338	30	2.25	1.5	400	84.83%

89	338	30	2.25	1.5	400	86.23%
90	338	30	2.25	1.5	400	91.82%
91	338	30	1.75	1.5	600	86.66%
92	338	30	1.75	1.5	600	86.66%
93	338	30	1.75	1.5	600	85.21%
94	338	30	2.25	1.5	600	87.15%
95	338	30	2.25	1.5	600	88.60%
96	338	30	2.25	1.5	600	92.96%
97	328	30	2	1.5	400	83.79%
98	328	30	2	1.5	400	86.59%
99	328	30	2	1.5	400	86.59%
100	348	30	2	1.5	400	93.40%
101	348	30	2	1.5	400	97.70%
102	348	30	2	1.5	400	91.96%
103	328	30	2	1.5	600	91.67%
104	328	30	2	1.5	600	94.51%
105	328	30	2	1.5	600	90.25%
106	348	30	2	1.5	600	96.67%
107	348	30	2	1.5	600	96.67%
108	348	30	2	1.5	600	98.08%
109	338	20	2	1.25	500	97.47%
110	338	20	2	1.25	500	98.90%
111	338	20	2	1.25	500	98.90%
112	338	40	2	1.25	500	97.34%
113	338	40	2	1.25	500	98.77%
114	338	40	2	1.25	500	95.91%
115	338	20	2	1.75	500	97.32%
116	338	20	2	1.75	500	98.80%
117	338	20	2	1.75	500	98.80%
118	338	40	2	1.75	500	85.70%
119	338	40	2	1.75	500	87.10%
120	338	40	2	1.75	500	89.88%
121	338	30	2	1.5	500	99.67%
122	338	30	2	1.5	500	96.84%
123	338	30	2	1.5	500	98.25%
124	338	30	2	1.5	500	99.12%
125	338	30	2	1.5	500	99.12%
126	338	30	2	1.5	500	99.12%
127	338	30	2	1.5	500	98.62%

128	338	30	2	1.5	500	99.99%
129	338	30	2	1.5	500	99.99%
130	338	30	2	1.5	500	98.98%
131	338	30	2	1.5	500	98.98%
132	338	30	2	1.5	500	98.98%
133	338	30	2	1.5	500	99.36%
134	338	30	2	1.5	500	99.36%
135	338	30	2	1.5	500	97.93%
136	338	30	2	1.5	500	97.87%
137	338	30	2	1.5	500	99.30%
138	338	30	2	1.5	500	99.30%
139	338	30	1.75	1.5	500	90.44%
140	338	30	1.75	1.5	500	87.65%
141	338	30	1.75	1.5	500	93.24%
142	298	50	2	2	0	65.34%
143	298	50	2	2	0	63.95%
144	298	50	2	2	0	65.07%
145	308	50	2	2	0	66.77%
146	308	50	2	2	0	71.00%
147	308	50	2	2	0	69.59%
148	318	50	2	2	0	75.23%
149	318	50	2	2	0	73.82%
150	328	50	2	2	0	75.94%
151	328	50	2	2	0	78.05%
152	328	50	2	2	0	79.47%
153	338	50	2	2	0	80.88%
154	338	50	2	2	0	82.76%
155	338	50	2	2	0	84.64%
156	338	50	2	2	0	83.70%
157	338	30	2	2	0	81.31%
158	338	30	2	2	0	84.19%
159	338	30	2	2	0	81.31%
160	338	40	2	2	0	79.87%

161	338	40	2	2	0	78.43%
162	338	40	2	2	0	79.87%
163	338	50	2	2	0	78.43%
164	338	50	2	2	0	78.43%
165	338	50	2	2	0	76.99%
166	338	60	2	2	0	76.99%
167	338	60	2	2	0	75.55%
168	338	60	2	2	0	75.55%
169	338	70	2	2	0	75.55%
170	338	70	2	2	0	74.11%
171	338	70	2	2	0	72.67%
172	338	30	1.5	2	0	78.36%
173	338	30	1.5	2	0	75.48%
174	338	30	1.5	2	0	78.36%
175	338	30	1.75	2	0	78.38%
176	338	30	1.75	2	0	78.38%
177	338	30	1.75	2	0	75.50%
178	338	30	2	2	0	81.31%
179	338	30	2	2	0	84.19%
180	338	30	2	2	0	81.31%
181	338	30	2.25	2	0	79.89%
182	338	30	2.25	2	0	78.45%
183	338	30	2.25	2	0	77.01%
184	338	30	2.5	2	0	75.50%
185	338	30	2.5	2	0	78.38%
186	338	30	2.5	2	0	79.82%
187	338	30	2	1.5	0	85.65%
188	338	30	2	1.5	0	84.21%
189	338	30	2	1.5	0	82.77%
190	338	30	2	1.75	0	82.75%
191	338	30	2	1.75	0	82.75%
192	338	30	2	1.75	0	84.19%
193	338	30	2	2	0	81.31%

194	338	30	2	2	0	84.19%
195	338	30	2	2	0	81.31%
196	338	30	2	2.25	0	79.84%
197	338	30	2	2.25	0	81.28%
198	338	30	2	2.25	0	81.28%
199	338	30	2	2.5	0	79.87%
200	338	30	2	2.5	0	78.43%
201	338	30	2	2.5	0	79.87%
202	338	30	2	1.5	0	81.31%
203	338	30	2	1.5	0	84.19%
204	338	30	2	1.5	0	81.31%
205	338	30	2	1.5	100	87.09%
206	338	30	2	1.5	100	85.65%
207	338	30	2	1.5	100	85.65%
208	338	30	2	1.5	200	87.07%
209	338	30	2	1.5	200	88.51%
210	338	30	2	1.5	200	88.51%
211	338	30	2	1.5	300	89.92%
212	338	30	2	1.5	300	92.80%
213	338	30	2	1.5	300	91.36%
214	338	30	2	1.5	400	92.83%
215	338	30	2	1.5	400	94.28%
216	338	30	2	1.5	400	92.83%
217	338	30	2	1.5	500	95.72%
218	338	30	2	1.5	500	94.28%
219	338	30	2	1.5	500	95.72%
220	298	30	2	1.5	0	54.22%
221	298	30	2	1.5	0	52.91%
222	298	30	2	1.5	0	52.91%
223	298	30	2	1.5	0	53.92%
224	298	30	2	1.5	0	55.90%
225	298	30	2	1.5	0	55.12%
226	298	30	2	1.5	0	56.70%

227	298	30	2	1.5	0	54.73%
228	298	30	2	1.5	0	55.70%
229	298	30	2	1.5	0	55.39%
230	298	30	2	1.5	0	57.31%
231	298	30	2	1.5	0	56.44%
232	298	30	2	1.5	0	58.81%
233	298	30	2	1.5	0	56.83%
234	298	30	2	1.5	0	57.88%
235	298	30	2	1.5	0	59.20%
236	298	30	2	1.5	0	57.25%
237	298	30	2	1.5	0	58.24%
238	308	30	2	1.5	0	61.10%
239	308	30	2	1.5	0	59.11%
240	308	30	2	1.5	0	60.15%
241	308	30	2	1.5	0	62.45%
242	308	30	2	1.5	0	60.48%
243	308	30	2	1.5	0	61.48%
244	308	30	2	1.5	0	63.50%
245	308	30	2	1.5	0	61.53%
246	308	30	2	1.5	0	62.53%
247	308	30	2	1.5	0	64.01%
248	308	30	2	1.5	0	62.04%
249	308	30	2	1.5	0	63.04%
250	308	30	2	1.5	0	64.99%
251	308	30	2	1.5	0	63.02%
252	308	30	2	1.5	0	64.02%
253	308	30	2	1.5	0	66.07%
254	308	30	2	1.5	0	64.10%
255	308	30	2	1.5	0	65.10%
256	318	30	2	1.5	0	64.33%
257	318	30	2	1.5	0	62.36%
258	318	30	2	1.5	0	63.36%
259	318	30	2	1.5	0	65.03%

260	318	30	2	1.5	0	63.06%
261	318	30	2	1.5	0	64.06%
262	318	30	2	1.5	0	66.05%
263	318	30	2	1.5	0	64.08%
264	318	30	2	1.5	0	65.08%
265	318	30	2	1.5	0	67.30%
266	318	30	2	1.5	0	65.33%
267	318	30	2	1.5	0	66.33%
268	318	30	2	1.5	0	68.39%
269	318	30	2	1.5	0	66.42%
270	318	30	2	1.5	0	67.42%
271	318	30	2	1.5	0	69.65%
272	318	30	2	1.5	0	67.68%
273	318	30	2	1.5	0	68.68%
274	328	30	2	1.5	0	67.63%
275	328	30	2	1.5	0	65.66%
276	328	30	2	1.5	0	66.66%
277	328	30	2	1.5	0	68.64%
278	328	30	2	1.5	0	66.67%
279	328	30	2	1.5	0	67.67%
280	328	30	2	1.5	0	69.30%
281	328	30	2	1.5	0	67.33%
282	328	30	2	1.5	0	68.33%
283	328	30	2	1.5	0	70.52%
284	328	30	2	1.5	0	68.55%
285	328	30	2	1.5	0	69.55%
286	328	30	2	1.5	0	71.18%
287	328	30	2	1.5	0	69.21%
288	328	30	2	1.5	0	70.21%
289	328	30	2	1.5	0	72.32%
290	328	30	2	1.5	0	70.35%
291	328	30	2	1.5	0	71.35%
292	338	30	2	1.5	0	72.15%

293	338	30	2	1.5	0	70.18%
294	338	30	2	1.5	0	71.18%
295	338	30	2	1.5	0	72.55%
296	338	30	2	1.5	0	70.58%
297	338	30	2	1.5	0	71.58%
298	338	30	2	1.5	0	73.10%
299	338	30	2	1.5	0	71.13%
300	338	30	2	1.5	0	72.13%
301	338	30	2	1.5	0	74.21%
302	338	30	2	1.5	0	72.24%
303	338	30	2	1.5	0	73.24%
304	338	30	2	1.5	0	75.75%
305	338	30	2	1.5	0	73.78%
306	338	30	2	1.5	0	74.78%
307	338	30	2	1.5	0	76.96%
308	338	30	2	1.5	0	74.99%
309	338	30	2	1.5	0	75.99%
310	298	30	2	1.5	500	68.22%
311	298	30	2	1.5	500	66.25%
312	298	30	2	1.5	500	67.25%
313	298	30	2	1.5	500	70.29%
314	298	30	2	1.5	500	68.32%
315	298	30	2	1.5	500	69.32%
316	298	30	2	1.5	500	72.20%
317	298	30	2	1.5	500	70.23%
318	298	30	2	1.5	500	71.23%
319	298	30	2	1.5	500	74.22%
320	298	30	2	1.5	500	72.25%
321	298	30	2	1.5	500	73.25%
322	298	30	2	1.5	500	76.74%
323	298	30	2	1.5	500	74.77%
324	298	30	2	1.5	500	75.77%
325	298	30	2	1.5	500	77.73%

326	298	30	2	1.5	500	75.76%
327	298	30	2	1.5	500	76.75%
328	308	30	2	1.5	500	70.02%
329	308	30	2	1.5	500	68.05%
330	308	30	2	1.5	500	69.06%
331	308	30	2	1.5	500	73.32%
332	308	30	2	1.5	500	71.35%
333	308	30	2	1.5	500	72.35%
334	308	30	2	1.5	500	75.45%
335	308	30	2	1.5	500	73.48%
336	308	30	2	1.5	500	74.48%
337	308	30	2	1.5	500	77.36%
338	308	30	2	1.5	500	75.39%
339	308	30	2	1.5	500	76.39%
340	308	30	2	1.5	500	78.72%
341	308	30	2	1.5	500	76.75%
342	308	30	2	1.5	500	77.75%
343	308	30	2	1.5	500	80.38%
344	308	30	2	1.5	500	78.41%
345	308	30	2	1.5	500	79.41%
346	318	30	2	1.5	500	71.73%
347	318	30	2	1.5	500	69.76%
348	318	30	2	1.5	500	70.77%
349	318	30	2	1.5	500	74.98%
350	318	30	2	1.5	500	73.01%
351	318	30	2	1.5	500	74.02%
352	318	30	2	1.5	500	76.58%
353	318	30	2	1.5	500	74.61%
354	318	30	2	1.5	500	75.61%
355	318	30	2	1.5	500	78.96%
356	318	30	2	1.5	500	76.99%
357	318	30	2	1.5	500	77.99%
358	318	30	2	1.5	500	80.72%

359	318	30	2	1.5	500	78.75%
360	318	30	2	1.5	500	79.75%
361	318	30	2	1.5	500	82.93%
362	318	30	2	1.5	500	80.96%
363	318	30	2	1.5	500	81.96%
364	328	30	2	1.5	500	73.39%
365	328	30	2	1.5	500	71.42%
366	328	30	2	1.5	500	72.42%
367	328	30	2	1.5	500	77.10%
368	328	30	2	1.5	500	75.13%
369	328	30	2	1.5	500	76.13%
370	328	30	2	1.5	500	79.19%
371	328	30	2	1.5	500	77.22%
372	328	30	2	1.5	500	78.22%
373	328	30	2	1.5	500	81.10%
374	328	30	2	1.5	500	79.13%
375	328	30	2	1.5	500	80.13%
376	328	30	2	1.5	500	82.96%
377	328	30	2	1.5	500	80.99%
378	328	30	2	1.5	500	81.99%
379	328	30	2	1.5	500	84.89%
380	328	30	2	1.5	500	82.92%
381	328	30	2	1.5	500	83.92%
382	338	30	2	1.5	500	75.90%
383	338	30	2	1.5	500	73.93%
384	338	30	2	1.5	500	74.93%
385	338	30	2	1.5	500	79.19%
386	338	30	2	1.5	500	77.22%
387	338	30	2	1.5	500	78.22%
388	338	30	2	1.5	500	81.22%
389	338	30	2	1.5	500	79.25%
390	338	30	2	1.5	500	80.25%
391	338	30	2	1.5	500	83.21%

392	338	30	2	1.5	500	81.24%
393	338	30	2	1.5	500	82.24%
394	338	30	2	1.5	500	85.78%
395	338	30	2	1.5	500	83.81%
396	338	30	2	1.5	500	84.81%
397	338	30	2	1.5	500	87.19%
398	338	30	2	1.5	500	85.22%
399	338	30	2	1.5	500	86.22%

Table S4. Comparison between BP-ANN Predicted Conditions and Experimental Sulfuration Efficiency.

Times	1	2	3	4	5	6
Predicted values	98.73%	98.73%	98.73%	98.73%	98.73%	98.73%
Actual values	97.82%	98.01%	97.56%	97.21%	98.33%	97.98%

Energy Inventory and Environmental Implication Assessment

To rigorously evaluate the industrial sustainability of the proposed "Ultrasound-Enhanced Transformation–Solid Phase Electrolysis" strategy, a gate-to-gate energy inventory analysis was conducted based on a functional unit of 1 ton of metallic lead (Pb) produced. While the laboratory-scale data confirm a significant reduction in electrolysis energy consumption (35.8%, from 879.96 to 565.08 $kWh \cdot t^{-1} \cdot Pb$), a holistic assessment must account for the auxiliary energy inputs introduced by the ultrasonic pretreatment and thermal regulation.

(1) Scale-up Assumptions and Energy Balance

Direct linear extrapolation of laboratory energy data (e.g., 600 W ultrasonic power for 10 g paste) often leads to overestimated values due to the low energy efficiency of probe-type sonication systems. For industrial implementation, we assume the deployment of mature large-scale sonochemical reactors with a specific energy consumption of approximately 80–100 $kWh \cdot m^3$. Furthermore, regarding the thermal requirement to maintain the reaction at 347.97 K, industrial hydrometallurgical circuits typically employ heat exchangers to recover waste heat from the exothermic acid dilution and the Joule heating of electrolytic cells. Assuming a conservative industrial heat recovery efficiency (η_{rec}) of 70%, the net thermal energy input for the pretreatment

stage is significantly mitigated.

(2) Decarbonization and technical advantages

Table S5 presents a comparative analysis of the proposed route against traditional pyrometallurgy and direct solid-phase electrolysis. Although the inclusion of pretreatment steps introduces an additional energy penalty, the total equivalent energy consumption of the proposed process remains competitive. Crucially, this strategy offers two decisive advantages that justify the thermodynamic trade-off:

(1) Elimination of Refractory Phases: By converting the mixed phases (PbO_2/PbO) into a unitary $PbSO_4$ precursor, the process eliminates the high overpotential and parasitic side reactions (e.g., oxygen evolution) associated with the direct electrolysis of PbO2. This ensures a stable current efficiency of 90.80% and a high lead recovery rate of 98.68%.

(2) Scope 1 Emissions Reduction: Unlike pyrometallurgical smelting, which relies on the combustion of coke and emits substantial CO_2 and lead dust, the proposed route is fully electrified. Quantitatively, traditional smelting emits approx. 0.4–0.6 tons of direct CO_2 per ton of lead (stoichiometrically derived from $2PbO + C \rightarrow 2Pb + CO_2$). By replacing carbon reduction with electron transfer ($PbSO_4 + 2e^- \rightarrow Pb + SO_4^{2-}$), this direct emission is mathematically reduced to zero in the proposed process. Although indirect emissions (Scope 2) depend on the grid mix, the elimination of the intrinsic carbon reductant represents a permanent decarbonization of the process chemistry. This shifts the carbon footprint from direct Scope 1 emissions to Scope 2 (electricity generation), offering a pathway to near-zero carbon emissions as industrial grids transition to renewable energy sources.

(3) Economic Implications (OPEX and CAPEX)

Economically, the framework offers a highly competitive Operational Expenditure (OPEX) profile. While the sonochemical pretreatment introduces front-end reagent costs for H_2O_2 and H_2SO_4, these expenses are structurally offset by the downstream electrical efficiency. The absolute energy saving of 314.88 $kWh \cdot t^{-1}$ Pb provides substantial and continuous cost mitigation at standard industrial electricity rates. Moreover, the $(NH_4)_2SO_4$ electrolyte acts as a stable, non-consumable supporting medium; after routine pH neutralization, it can be continuously recycled, minimizing ongoing chemical makeup costs. From a Capital Expenditure (CAPEX) perspective, this low-temperature hydrometallurgical route circumvents the need for massive investments in high-temperature rotary furnaces and the stringent off-gas treatment

infrastructure (e.g., desulfurization scrubbers and lead dust baghouses) mandated for conventional pyrometallurgy. This integrated approach thus presents a compelling, quantified economic case for scalable secondary lead recovery.

Table S5. Comparative estimation of technical and environmental indicators for 1 ton of Pb production.

Indicator	Pyrometallurgical Smelting	Direct Solid-Phase Electrolysis	This Work (Ultrasonic-Enhanced)
Primary Energy Source	Coke/Coal + Electricity	Electricity	Electricity
Reaction Temperature	>1273 K	Ambient (298 K)	347.97 K (Pretreatment) + Electrolysis
Electrolysis Energy ($kWh \cdot t^{-1} \cdot Pb$)	N/A (Refining step only)	879.96	565.08
Product Purity & Morphology	Lead Bullion (Requires refining)	Sponge Pb (Risk of PbO_2 inclusion)	High-Purity Sponge Pb
Direct CO_2 Emissions	High (Carbothermal reduction)	Low	Negligible
Process Stability	Mature but high pollution	Unstable (Anode passivation)	High (Unitary phase precursor)

In conclusion, although the ultrasonic pretreatment introduces an energy penalty, the sharp decrease in electrolysis specific energy consumption (SEC) and the superior product quality justify the trade-off. The process offers a technically viable pathway to electrify the lead recycling industry, aligning with carbon neutrality mandates. Nevertheless, we acknowledge that the current assessment is based on theoretical scale-up assumptions. The precise quantification of specific energy consumption for the pretreatment unit, particularly the optimization of heat recovery efficiency and ultrasonic reactor design at the pilot scale, remains a critical objective for our future research.

Experimental sections

Materials and chemical reagents

All chemicals used in this study were of analytical grade. H_2SO_4 was purchased from Chongqing Chuandong Chemical Co., Ltd., and H_2O_2 was obtained from Chengdu cologne chemicals Co., Ltd. All aqueous solutions were prepared using ultrapure water (Millipore, ≥18 MΩ·cm).

The SLP used in this work was supplied by Yunnan Xiangyun Feilong recycling technology Co., Ltd. Prior to experiments, the SLP was ground for 6 hours using a planetary ball mill (MITR, YXQM-2L), dried, and sieved through a 200-mesh screen to obtain a homogeneous powder.

Ultrasound-assisted phase conversion

The phase transformation was performed in a thermostated acoustic reactor. Pretreated SLP powder (10 g) was dispersed in 150 mL of distilled water. The stoichiometry was rigorously controlled by adding 10 wt.% H_2O_2 (molar ratio H_2O_2/Pb^{4+}) and 10% dilute H_2SO_4 (molar ratio H_2SO_2/Pb^{2+}) to prevent premature precipitation. The slurry was subjected to ultrasonic irradiation (19.48 kHz) at variable powers (0–800 W) for 2 h. post-reaction, the solid residue was filtered, washed to neutrality, and dried for compositional analysis. The conversion efficiency (w) was quantified using Eq. (1). A schematic of the SLP transformation process is shown in **Figure S6**.

$$w = \frac{m_2 - m_1}{m - m_1} \times 100\% \quad (1)$$

where w represents the conversion efficiency of Pb in SLP (%), m is the mass of SLP used (g), m_1 is the mass of $PbSO_4$ contained in the SLP (g), and m_2 is the mass of the recovered $PbSO_4$ (g).

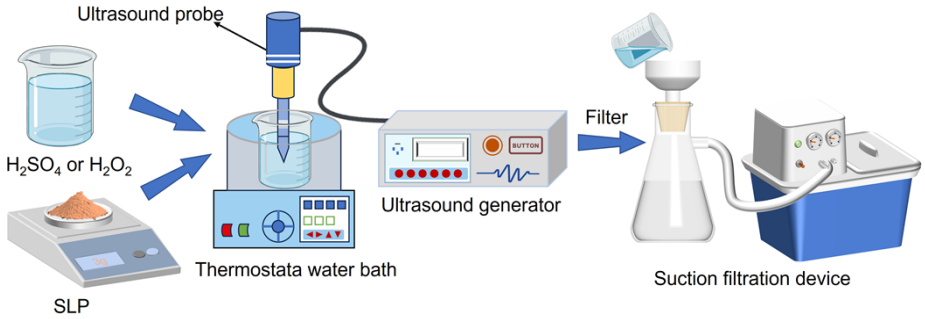

Figure S3. Illustration of conversion process of SLP.

Solid phase electroreduction

SLP cathodes were prepared on lead-based grids using a conventional coating

method. First, 10 g of sulfured SLP from the previous step was dry-mixed with short cellulose fibers in a mortar for 30 min. An appropriate amount of deionized water was then added, and the mixture was stirred for 5 min to form a homogeneous slurry. The SLP mixture was uniformly coated onto grid-shaped lead plates (40 mm × 28 mm × 1 mm) using a stainless-steel blade to level the surface, and the coated cathodes were dried in a vacuum oven at 80 °C for 8 h.

The anodes consisted of Ti plates coated with Sn-Sb (40 mm × 30 mm × 1 mm, Ti/SnO_2-Sb_2O_3). The Ti substrate was first roughened via sandblasting to enhance coating adhesion, followed by acid etching in a HCl mixture ($V_{HF}/V_{HNO3}/V_{H2O}$ = 1:4:5) to remove the oxide layer and improve surface cleanliness. Multi-layer nanoscale Sn-Sb coatings were then applied through multiple quantitative coatings and high-temperature sintering.

Solid-phase electrolysis experiments were performed in an electronically controlled thermostatic water bath using a HHB17301SL DC power supply to regulate cathodic current density. The electrolysis employed an electrolyte of 200 g/L $(NH_4)_2SO_4$ and a current density of 200 A/m^2, utilizing an SLP cathode and a Ti/SnO_2-Sb_2O_3 anode positioned 50 mm apart. During electrolysis, the cell voltage was recorded over time, and changes in the cathode surface were observed. Electrolysis was terminated when a sharp rise in cell voltage accompanied by vigorous H_2 evolution indicated completion. The cathode was then removed, thoroughly washed, and dried under vacuum to prevent lead oxidation. A schematic of the SLP solid-phase electrolysis setup is shown in **Figure S4**.

The key parameters of the Solid-phase electrolysis process were calculated as follows：

The average cell voltage ($\overline{U}$) was determined using the following equation:

$$\overline{U} = \int \frac{Udt}{t} \tag{2}$$

In the equation, U(V) represents the real-time cell voltage, and t (s) is the electrolysis time.

The charge required to process one ton of Pb (Q_0, C·t^{-1} Pb) was calculated as follows:

$$Q_0 = \frac{\Delta Q}{\Delta m} = \frac{\int IAdt}{m} \times 10^3 \tag{3}$$

In the equation, I(mA/cm^2) is the current density, A(cm^2) is the electrode area, and

m(g) is the mass of metallic Pb, determined by weighing.

The energy consumption (E_0, kWh·t-1·Pb·) of the Solid-phase electrolysis process was calculated according to Eq. (4):

$$E_0 = \frac{\Delta E}{\Delta m} = \frac{1}{3600} \cdot \frac{\int UIAdt}{m} = \frac{1}{3.6 \times 10^6} \cdot \overline{U} \cdot Q_0 \quad (4)$$

The cathodic current efficiency (η,%) of the Solid-phase electrolysis was calculated using Eq. 5:

$$\eta = \frac{m/M_{Pb}}{\Delta Q/(zF)} \times 100\% = \frac{zF}{M_{Pb}Q_0} \times 100\% \quad (5)$$

In the equation, F is the Faraday constant (F=96485 C·mol^{-1}), M_{Pb} is the molar mass of Pb (M_{Pb}=207 g·mol^{-1}), and z is the number of electrons required to obtain a Pb atom, where m(g) is the mass of metallic Pb obtained, m_0(g) is the mass of the original SLP coated on the cathode, and λ_0 (wt.%) is the Pb content in the original SLP, determined by EDTA titration.

$$\varepsilon = \frac{m}{\lambda_0 m_0} \times 100\% \quad (6)$$

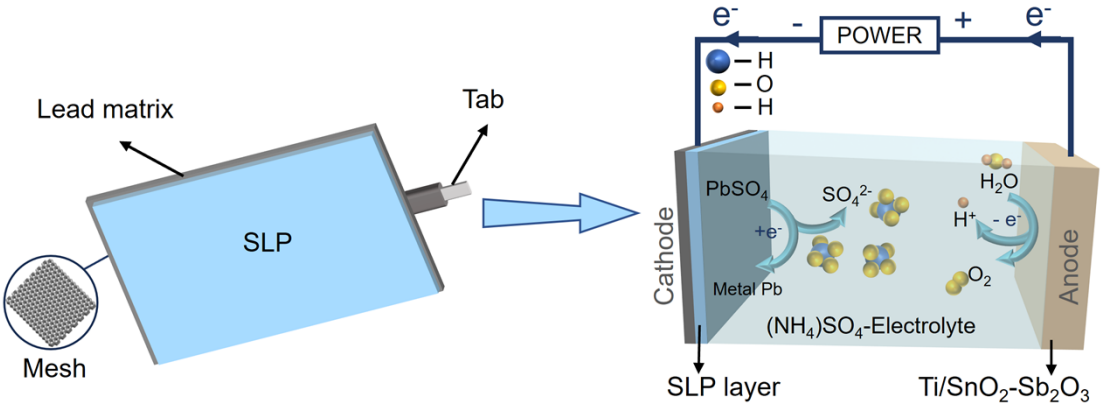

Figure S4. The process of solid-phase electrolysis

Physical characterization

X-ray diffraction (XRD) patterns were collected on an Empyrean-100 (PANalytical, Netherlands) diffractometer equipped with a Cu Kα radiation source (λ = 1.5406 Å) operating at 40 mA and 40 kV. The microstructure of all samples was observed with a JSM-7900F field emission scanning electron microscope (SEM) with energy dispersive spectroscopy (EDS). X-ray photoelectron spectroscopy (XPS) tests were carried out on the Thermo fisher Escalab 250 Xi+ (Thermofisher, USA), Multipak software was employed to fit the XPS data. The C 1s peak at 284.8 eV was commonly used as a reference for charge correction.

Computational methods

First-principles calculations based on Density Functional Theory (DFT) were performed to elucidate the electronic structure and bonding characteristics of lead species. The calculations were carried out using the Vienna Ab initio Simulation Package (VASP). The detailed parameters, including the exchange-correlation functional, cutoff energy, and k-point sampling, are provided following:

All Density Functional Theory (DFT) calculations were performed using the Vienna Ab initio Simulation Package (VASP) [1,2]. The projector augmented wave (PAW) method was employed to describe the ion-electron interactions [3]. The exchange-correlation energy was treated within the Generalized Gradient Approximation (GGA) using the Perdew-Burke-Ernzerhof (PBE) functional [4].

For the structural optimization and electronic property calculations of PbO_2 (rutile), PbO (litharge), and $PbSO_4$ (anglesite), a plane-wave basis set with a cutoff energy of 500 eV was used. The Brillouin zone was sampled using the Monkhorst-Pack scheme with a grid density of $4 \times 4 \times 4$ for bulk calculations [5]. The convergence criteria for energy and force were set to 10^{-5} eV and 0.02 eV/Å, respectively.

To analyze the bonding characteristics, the Density of States (DOS) and Band Structure were calculated. The Electron Localization Function (ELF) and Differential Charge Density (DCD) were visualized using the VESTA software to qualitatively distinguish between the covalent and ionic bonding nature of the lead compounds [6].

References:

[1] G. Kresse, J. Furthmüller, Phys. Rev. B 54 (1996) 11169.

[2] G. Kresse, D. Joubert, Phys. Rev. B 59 (1999) 1758.

[3] P.E. Blöchl, Phys. Rev. B 50 (1994) 17953.

[4] J.P. Perdew, K. Burke, M. Ernzerhof, Phys. Rev. Lett. 77 (1996) 3865.

[5] H.J. Monkhorst, J.D. Pack, Phys. Rev. B 13 (1976) 5188.

[6] K. Momma, F. Izumi, J. Appl. Crystallogr. 44 (2011) 1272.